1

Development of an improved two-sphere integration technique for quantifying black carbon concentrations in the atmosphere and seasonal snow

Xin Wang [1,2], **Xueying Zhang** [3] and **Wenjing Di** [1]

[1] Key Laboratory for Semi-Arid Climate Change of the Ministry of Education, Lanzhou University,

  Lanzhou 730000, Gansu, China

[2] Institute of Surface-Earth System Science, Tianjin University, Tianjin 300072

[3] Jilin Weather Modification Office, Changchun 132000, Jilin, China

Correspondence to: Xin Wang (Tel: +86 931 8915892)

   E-mail address: wxin@lzu.edu.cn   (X. Wang)

Submitted on August 2019

Abstract. An improved two-sphere integration (TSI) technique has been developed to quantify black carbon (BC) concentrations in the atmosphere and seasonal snow. The major advantage of this system is that it combines two distinct integrated-spheres to reduce the scattering effect due to light-absorbing particles, and thus provides accurate determinations of total light absorption from BC collected on Nuclepore filters. The TSI technique can be calibrated using a series of 15 filter samples of standard fullerene soot. This technique quantifies the mass of BC by separating the spectrally resolved total light absorption into BC and non-BC fractions. To assess the accuracy of the improved system, an empirical procedure for measuring BC concentrations by a two-step thermal–optical method is also applied. Laboratory results indicate that BC concentrations determined using the TSI technique and theoretical calculations are well correlated (R^2=0.99), whereas the thermal–optical method underestimates BC concentrations by 35%–45% than that measured by TSI technique. Assessments of the two methods for atmospheric and snow samples revealed excellent agreement, with least-squares regression lines with slopes of 1.72 ($r^2 = 0.67$) and 0.84 ($r^2 = 0.93$), respectively. However, the TSI technique is more accurate in quantifications of BC concentrations in both the atmosphere and seasonal snow, with an overall lower uncertainty. Using the improved TSI technique, we find that light absorption at a wavelength of 550 nm due to BC plays a dominant role, relative to non-BC light absorption, in both the atmosphere (62.76%–91.84% of total light absorption) and seasonal snow (43.11%–88.56%) over northern China.

1 Introduction

Black carbon (BC) has long been recognized as the major light-absorbing particles (LAPs) in both natural and anthropogenic emissions (Slater et al., 2002; Koch et al., 2009; Zhang et al., 2009; Pan et al., 2010; McMeeking et al., 2011; Pavese et al., 2012; Bond et al., 2013; IPCC, 2013). BC can impact the regional and global climate in several ways, including via the direct effects of scattering and absorbing visible solar radiation (Jacobson, 2001b; Menon et al., 2002; Hansen et al., 2005; Ramanathan and Carmichael, 2008), the semi-direct effects of changing the temperature structure and relative humidity of the atmosphere by absorbing solar short-wave radiation (Weiss et al., 2012), and indirect effects on cloud formation and lifetime (Chuang et al., 2002; Baumgardner et al., 2004; Rosenfeld et al., 2008). Once deposited onto snow or ice surfaces, BC absorbs more solar radiation than pure snow or ice and reduces the snow albedo, thus accelerating snow melt (Xu et al., 2009a; Flanner et al., 2012; Hadley and Kirchstetter, 2012; Carmagnola et al., 2013; Qian et al., 2014; Zhao et al., 2014).

Optically classified BC is also often referred to as elemental carbon (EC), which is typically thermally detected. The distinction between BC and EC has been debated since the 1980s (Heintzenberg, 1989; Horvath, 1993a; Andreae and Gelencser, 2006; Moosmuller et al., 2009). Given that BC and EC are both soot particles with diameters of <1 μm, these terms have often been used interchangeably (Chow et al., 2001, 2004; Ming et al., 2009; Thevenon et al., 2009; Lim et al., 2014). BC is generally regarded as ideal light-absorbing particles of carbon, and is typically measured using optical attenuation methods (Clarke et al., 1987; Grenfell et al., 2011; Hansen et al., 1984; Ogren and Charlson, 1983). The term 'EC' is often used interchangeably with 'BC' when referring to optical absorption measurements (Clarke et al., 1987; Grenfell et al., 2011), and is only uniquely identified by thermal–optical methods (Xu et al., 2006; Cao et al., 2007; Jimenez et al., 2009). There remains poor agreement between measurements of BC and EC among available measurement techniques. The general techniques used to quantify the various fractions of BC mass concentrations are associated with the corresponding methods: thermal–optical methods, single-particle soot photometer (SP2) measurements, and filter-based optical techniques. Besides the above techniques, the aerosol mass

spectrometry, electron microscopy, and Raman spectroscopy are also useful and accurate methods to identify the various fractions of carbonaceous aerosols in the atmosphere (Cross et al., 2010; Ivleva et al., 2007; Spencer et al., 2007; Li et al., 2016; Petzold et al., 2013). Among these methods, the thermal–optical approach is regarded as the most effective and reliable for evaluating EC concentrations (Chylek et al., 1987; Cachier and Pertuisot, 1994; Jenk et al., 2006; Legrand et al., 2007; Hadley et al., 2010). However, the thermal–optical method can lead to large discrepancies in determining EC concentrations as a result of inference from positive artifacts caused by inadequately separated organics and mineral dust (Ballach et al., 2001; Wang et al., 2012). Further discrepancies are caused by the use of two main detection protocols [thermal–optical transmission (TOT) and thermal–optical reflectance (TOR)] to assess EC and OC concentrations based on their unique thermal properties. These protocols yield different OC and EC concentrations (Chow et al., 1993, 2001; Birch and Cary, 1996; Watson and Chow, 2002). The Integrating Sphere/Integrating Sandwich Spectrophotometer (ISSW) method was developed by Grenfell et al. (2011) and has been used to analyze mass concentrations of BC in snow (Doherty et al., 2010, 2014; Wang et al., 2013). Doherty et al. (2010) noted that the total uncertainty in measuring BC in snow using the ISSW method is up to 40% relative to the gravimetric standards of BC (fullerene soot). The total uncertainty associated with the filter-based ISSW technique on BC concentration determination for ambient snow has previously been estimated as 40 %, which is the sum, in quadrature, of 11% for instrumental uncertainty, 15% for undercatch uncertainty (loss of insoluble light-absorbing impurities), 17% for BC mass absorption coefficient (MAC) uncertainty, and 30% for uncertainty in the AAE of non-BC material (Doherty et al., 2010; Grenfell et al., 2011; Schwarz et al., 2012). Finally, the SP2 technique is well suited to the quantification of low BC concentrations with small particle radius (<500 nm). It is an optimized method for measuring BC concentrations and size distributions, and the substantially larger uncertainty of the SP2 instrument with respect to BC concentration measurements can exceed 60% in snow and ice cores, and 30% for atmospheric sampling (Schwarz et al., 2012). They noted that the relative transmission efficiencies of polystyrene latex sphere concentration standards (PSLs) in liquid to the SP2 after

112   aerosolization remarkably reduce to 20% due to larger diameter of BC particles (> 500

113   nm). Therefore, the larger diameter of BC (>500 nm) is hardly captured by SP2

114   instrument with a collison-type nebulizer. Moreover, the mixing status of BC in snow is

115   more complicated than the standard fullerene soot in the laboratory and the typical BC in

116   the atmosphere.

117   Although several field campaigns have collected atmospheric, snow, and ice core

118   samples to measure BC and EC concentrations globally (Wolff and Cachier, 1998; von

119   Schneidemesser et al., 2009; Doherty et al., 2010, 2014; Ming et al., 2010; Huang et al.,

120   2011; Xu et al., 2012; Cong et al., 2015), biases remain in determinations of BC

121   concentrations, as is evident from a comparison among the results obtained with the SP2,

122   ISSW, and thermal–optical methods (Schwarz et al., 2012; Lim et al., 2014). As a result,

123   it is difficult to assess the effects of BC and EC on recent climate change using different

124   techniques, even in the same area.

125   Here we report the development of a new portable and accurate spectrophotometric

126   method based on the two-sphere integration (TSI) technique that can be used to

127   determine BC concentrations in both the atmosphere and seasonal snow. The improved

128   TSI technique minimizes scattering effects related to BC and non-BC insoluble particles

129   collected on Nuclepore filters, and thus provides a simple and accurate means to assess

130   BC concentrations in the atmosphere and seasonal snow. To assess the accuracy of the

131   new technique, a two-step thermal–optical method is applied to determine BC

132   concentrations on individual quartz fiber filters. Finally, we investigate the spatial

133   distribution of BC concentrations and the relative light absorption of surface snow over

134   northeast China. We also analyze the diurnal variations of BC in the atmosphere during

135   day and night over Lanzhou in northwest China.

136   **2   Experimental Procedures**

137   **2.1   Sampling sites and snow-sample filtration**

138   During the study period, less snow fell in 2014 than in 2010, and no seasonal snow was

139   present in the western part of Inner Mongolia. Therefore, we collected 94 snow samples

140 at 14 sites in January and February of 2014 across north China following the sampling
141 route of Huang et al. (2011). The sites are numbered in chronological order from 90 to
142 103, following previous snow surveys (Ye et al., 2012; Wang et al., 2013). Figure 1
143 shows the locations of the snow field campaigns across northern China. The sampling
144 locations were selected to be at least 50 km from any settlement and 1 km from the
145 nearest road. Snow samples were kept frozen before being filtered. We set up a
146 temporary laboratory along the sampling route. Owing to BC in snow is often
147 hydrophobic, long time melting could lose more BC to the container walls instead of
148 collected on the filter (Ogren et al., 1983). In order to minimize the loss of insoluble
149 ILAPs, we quickly melted the snow samples in a microwave within a very short time.
150 Therefore, the loss of insoluble LAPs is very limited, and can be neglectable. At present,
151 this method is widely performed for snow melting procedure. (Dothery et al., 2010, 2014;
152 Wang et al.,2013). Subsequently, we simultaneously filtered the snow samples using
153 quartz fiber filters with 1-μm pores and Nuclepore filters with 0.4-μm pores. Then, we
154 refiltered the snow samples for the quartz fiber filters using Nuclepore filters with 0.4-μm
155 pores to account for the loss of BC mass in the 1-μm pore quartz fiber filters. Finally, we
156 stored the original and refiltered snow samples in clean high-density polyethylene bottles
157 in a freezer at −30°C for subsequent analysis. For details of the sampling and filtration
158 procedures, see Wang et al. (2013).

159 To evaluate the accuracy of the TSI technique in measuring BC concentrations, the
160 atmospheric samples were collected continuously on Nuclepore and quartz fiber filters
161 with high-volume samplers during the periods 09:00 to 17:00 (daytime; local time) and
162 23:00 to 07:00 (nighttime) at site 103 in Lanzhou from 5 to 25 August 2015. The pumps
163 were operated at a flow rate of 10 L min^{-1}. In total, 40 atmospheric samples were
164 collected during this experiment and used to assess the accuracy of the atmospheric BC
165 concentration measurements of the improved TSI technique.

166 **2.2   Two-sphere integration technique**

167 Light transmission techniques are the most commonly used methods for determining
168 light-absorbing impurities in aerosol filter samples of the atmosphere and snow/ice. Since
169 the 1970s, a series of optical attenuation techniques have been developed for estimating

170   BC concentrations using light transmission changes through filters, based on Beer's law.
171   An integrating sphere (IS) technique was first proposed for measuring BC by Fischer
172   (1970). The integrating sphere was coated with diffusely reflecting white paint through a
173   small hole, and the reduction in signal after measuring the sample filters represented the
174   absorption of BC. Subsequently, a new integrating plate (IP) instrument was developed to
175   measure scavenging BC on filters based on the IS technique, which uses a light-diffusing
176   support to provide a nearly Lambertian light source for light transmission using 0.4-μm
177   Nuclepore filters (Clarke et al., 1987; Horvath, 1993b). However, the multiple scattering
178   of solar radiation affect the accuracy of the IP technique (Clarke et al., 1987;
179   Hitzenberger, 1993; Petzold et al., 1997; Bond et al., 1999). A new integrating-sandwich
180   configuration of the ISSW instrument was designed to measure the absorption of
181   light-absorbing impurities based on the ISSW principle of Grenfell et al. (2011). The
182   ISSW instrument can isolate the absorption properties of light-absorbing impurities
183   deposited on polycarbonate Nuclepore filters. By assuming the mass absorption
184   efficiency and non-BC Ångström exponent at 550 nm, this technique is currently capable
185   of reliably measuring BC and non-BC light absorption (Wang et al., 2013; Dang and
186   Hegg, 2014; Doherty et al., 2014). However, Schwarz et al. (2012) found that the total
187   instrumental uncertainty associated with ISSW BC concentration determinations for
188   ambient snow is 11%, and that this uncertainty is partially due to the scattering effects of
189   insoluble impurities deposited on the filters (Doherty et al., 2010; Grenfell et al., 2011).

190   The improved TSI spectrophotometer developed in this study is small, lightweight, and
191   portable, and can accurately quantify BC concentrations using a technique based on the
192   integrating sphere and integrating plate transmission techniques (Fig. 2). The major
193   improvement of this spectrophotometer is that we replaced the integrating sandwich of
194   the ISSW instrument developed by Grenfell et al. (2011) with a new integrating sphere.
195   In addition, an iron hoop is applied to the top integrating sphere surrounding the sapphire
196   windows to reduce light scattering due to insoluble particles on the filters. Therefore, the
197   total relative light absorption due to all insoluble impurities on the filter can be estimated
198   from the visible-to-near-infrared wavelengths. The total light attenuation can be
199   calculated from the light transmitted by a snow or atmospheric sample, $S(\lambda)$, compared

with that transmitted by a blank filter, $S_0(\lambda)$. Then, the relative attenuation (Atn) through the filter can be expressed as follows

$$Atn = -\ln[S(\lambda)/S_0(\lambda)] \tag{1}$$

Then, the total absorption Ångström exponent $Å_{tot}(\lambda_0)$ of all the ILAPs on the filters can be calculated from the following formula:

$$Å_{tot}(\lambda_0) = -\frac{\ln[\tau_{tot}(\lambda_1)/\tau_{tot}(\lambda_2)]}{\ln(\lambda_1/\lambda_2)} \tag{2}$$

$Å_{non-BC}$ is calculated as a linear combination of the contributions to light absorption made by OC and Fe:

$$Å_{non-BC} = Å_{OC} \times f_{OC} + Å_{Fe} \times f_{Fe} \tag{3}$$

The total absorption Ångström exponent of all ILAPs on a filter ($Å_{tot}$) can be described as a linear combination of $Å_{BC}$ and $Å_{non-BC}$ weighted by the light absorption fraction:

$$Å_{tot}(\lambda_0) = Å_{BC} \times f_{BC}(\lambda_0) + Å_{non-BC} \times f_{non-BC}(\lambda_0) \tag{4}$$

Using the mass absorption efficiency and absorption Ångström exponents for BC, OC, and Fe described by Wang et al. (2013), we can further estimate the following parameters: equivalent BC (C_{BC}^{equiv}), maximum BC (C_{BC}^{max}), estimated BC (C_{BC}^{est}), fraction of light absorption by non-BC ILAPs (insoluble light-absorbing particles) (f_{non-BC}^{est}), absorption Ångström exponent of non-BC ILAPs ($Å_{non-BC}$), and total absorption Ångström exponent ($Å_{tot}$). These parameters are defined as follows.

1. C_{BC}^{equiv} (ng g^{-1}): *equivalent BC* is the amount of BC that would be needed to produce the total light absorption by all insoluble particles in snow for wavelengths of 300–750 nm.

2. C_{BC}^{max} (ng g^{-1}): *maximum BC* is the maximum possible BC mixing ratio in snow, assuming that all light absorption is due to BC at wavelengths of 650–700 nm.

3. C_{BC}^{est} (ng g^{-1}): *estimated BC* is the estimated true mass of BC in snow derived by separating the spectrally resolved total light absorption and non-BC fractions.

4. f_{non-BC}^{est} (%): the *fraction of light absorption by non-BC light-absorbing particles* is the integrated absorption due to non-BC light-absorbing particles. This value is weighted by the down-welling solar flux at wavelengths of 300–750 nm.

229 5. $Å_{non-BC}$: the *non-BC absorption Ångström exponent* is derived from the light absorption

230 by non-BC components for wavelengths of 450–600 nm.

231 6. $Å_{tot}$: the *absorption Ångström exponent* is calculated for all insoluble particles

232 deposited on the filter between 450 and 600 nm.

233   Furthermore, combining with the mass loading of Fe was determined by chemical

234 analysis (Wang et al., 2013), the mass loading of OC (L_{OC}) was also estimated assuming

235 that the MAC for OC is 0.3 $m^2 \, g^{-1}$ at the wavelength of 550 nm using the following

236 equation:

237 $$\tau_{tot}(\lambda) - MAC_{BC}(\lambda) \times L_{BC}^{est} - MAC_{Fe} \times L_{Fe} = MAC_{OC} \times L_{OC} \qquad (5)$$

238   All relevant equations and associated derivations are described by Grenfell et al. (2011)

239 and Doherty et al. (2010, 2014). Note that the calculation of non-BC light absorption due

240 to insoluble impurities assumes that the iron in snow is predominantly from mineral dust

241 (Wang et al., 2013).

242 **2.3 Calibration of the TSI spectrophotometer**

243   In this study, a series of 15 Nuclepore filters with a pore size of 0.2 μm (LOT#

244 7012284, 25mm, Whatman) loaded with fullerene soot (stock #40971, lot #L20W054,

245 Alfa Aesar, Ward Hill, MA, USA) is used to calibrate the spectrophotometer over the

246 range 0.63–38.6 μg, which typically covers >75% of ambient accumulation mode mass

247 (left panel in Table 1; Schwarz et al., 2012). Fullerene soot is commonly used for

248 calibrating the light transmission and thermal–optical techniques for measuring BC

249 concentrations (Baumgardner et al., 2012). Standard fullerene soot particles are

250 fractal-like aggregates of spherical primary particles with a diameter of ~50 nm, with a

251 mean density of 1.05 $g \, cm^{-3}$ (Moteki et al., 2009). Multiple filters with various loadings

252 are required, as the system response deviates from Beer's law exponential behavior;

253 related equations can be found in Grenfell et al. (2011). Note that uncertainties in mass

254 absorption efficiencies, which range from 2 to 25 $m^2 \, g^{-1}$, can lead to uncertainty in this

255 technique. Here, we use a mass absorption efficiency of 6.22 $m^2 \, g^{-1}$ at 525 nm, which is

256 consistent with Doherty et al. (2010) and Grenfell et al. (2011). Figure 3 shows the

257 best-fit curve (solid line) of loading of the filters at 550 nm. When the filter loading was

258   0–40 $\mu g\,cm^{-2}$, all measured results were close to the best-fit curve, indicating that the TSI

259   spectrophotometer is stable and accurate in terms of BC mass measurements.

2.4   Thermal−optical measurements of EC concentration

261   There are several types of thermal–optical method that can be used to quantify EC and

262   OC concentrations, including two-step temperatures in oxidizing/non-oxidizing

263   atmospheres (Cachier et al., 1989; Xu et al., 2006, 2009b), thermal–optical reflectance

264   (Chow et al., 1993, 2001; Chen et al., 2004), and thermal–optical transmittance (Sharma

265   et al., 2002; Yang and Yu, 2002; Chow et al., 2004). Using an optimized two-step

266   method, Cachier et al. (1989) first confirmed that soot carbon not only comprises EC, but

267   is also mixed with highly condensed organic material. An optimized two-step thermal–

268   optical system has been developed to detect EC and OC concentrations in ice cores (Xu

269   et al., 2006). Here, we use the optimized two-step method based on the thermal–optical

270   technique to measure EC concentrations. In this experiment, quartz fiber filters were first

271   preheated in a muffle furnace at 350°C to remove organic carbon prior to sampling. All

272   filters were punched to yield appropriately sized samples for analysis. Snow samples

273   were analyzed for EC and OC concentrations using a Thermal–Optical Carbon Analyzer

274   (Desert Research Institute, Model 2001A), following the thermal–optical reflectance

275   (TOR) protocol of the Interagency Monitoring of Protected Visual Environments

276   (IMPROVE_A). We developed a new method, referred to as the two-step method, to

277   measure the concentrations of BC collected by the quartz fiber filters. The two-step

278   method is an updated measurement procedure that first extracts an OC fraction below

279   550°C in a He atmosphere. The volatilized OC is oxidized to CO_2, reduced to CH_4, and

280   detected by a flame ionization system. Next, two EC fractions (EC1 and EC2) are

281   extracted above 550°C in an atmosphere of 2% O_2 and 98% He. Detailed procedures can

282   be found in Xu et al. (2006) and Chow et al. (2004). The analytical uncertainty of this

283   method is 15% for BC and 16% for OC measured via four parallel ice samples cut

284   lengthways in an ice core with high dust loading (Xu et al., 2009a).

3   Results

3.1 Comparison with theoretical calculations

To further assess the accuracy of the TSI system, we use standard fullerene soot and quantify BC concentrations using theoretical calculations for comparison with BC values measured by a laboratory-based TSI spectrophotometer. To ensure the stability and accuracy of the improved TSI spectrophotometer, two individual sets of standard BC filters were used: 0.4-μm Nuclepore and 1-μm quartz fiber filters. All filters were preheated in a muffle furnace at 350°C to remove organic carbon prior to sampling. A measured amount of BC was mixed into a known volume of ultrapure water. The mixture was then agitated by ultrasound for ~10 min, and the same volumes of liquid were then filtered through the two types of filter. Using the calculated BC mass, seven filters with gradually increasing BC concentrations were obtained for both the 0.4-μm Nuclepore and 1-μm quartz fiber filters. Next, all the filters were placed in a dryer for 24 h and then measured using the TSI spectrophotometer. Using the BC mass and the volume of the ultrapure water used for filtration, we can estimate the theoretical BC concentration for each filter. The mass for each filter is listed in Table 1 (right panel).

Assuming a mass absorption cross-section (MAC) of BC of 6.22 m^2 g^{-1} at 525 nm, the BC concentrations measured using the TSI spectrophotometer were in good agreement with the theoretical BC values in the slope of 1.07 (Figure 4). The BC mass loaded on the Nuclepore filters was approximately equal to that measured by the improved TSI spectrometer, which indicates that the TSI system developed here can accurately measure BC concentrations with the assumed mass absorption efficiency. In contrast, the standard BC mass on the quartz fiber filters was underestimated by 35%–45% using the two-step thermal–optical technique, compared with the theoretical value. During the filtration process, we found that the time required to filter liquid snow samples on the 0.4-μm Nuclepore filters was much longer than was the case for the 1-μm quartz fiber filters. Therefore, we first filtered the melted snow samples on the quartz fiber filters, and then re-filtered the snow samples using the 0.4-μm Nuclepore filters. Using this process, BC mass losses can be obtained using the TSI technique, assuming optical BC is equivalent to thermal EC.

315   As shown in Figure 5, the fraction of BC mass collected during the second filtration

316   (0.4-μm filter) ranges from 12% to 21% of the total collected mass (filter directly with

317   0.4-μm filters), as might be expected for the small particles of standard fullerene soot

318   (<50 nm). This under-sampled fraction decreases with increasing BC mass on the filters,

319   possibly owing to blocking of the filter pores. As a result, the under-sampled fraction of

320   the thermal–optical method was larger than that of the TSI technique, leading to a lower

321   filtration efficiency. Note that these sampling efficiencies are strongly related to the BC

322   size distribution. Therefore, the improved TSI technique developed here is more stable

323   and accurate for measuring pure BC masses, and the data obtained using this method can

324   be used as the standard BC mass. After correcting for systematic biases, the results of

325   both methods were closer to the theoretical BC calculations. Note, however, that the size

326   distribution of the laboratory BC standard was much smaller than those of the

327   atmospheric and seasonal snow samples (Schwarz et al., 2012). Therefore,

328   underestimates caused by the filtration efficiency for ambient BC should be lower than

329   that for the standard BC.

330   **3.2 Comparison of BC concentrations in seasonal snow and the atmosphere**

331   Recent studies have indicated that mineral dust can affect the accurate detection of BC

332   concentrations using the ISSW and thermal–optical methods (Wang et al., 2012; Zhou et

333   al., 2017). To eliminate the large uncertainty and bias due to dust particles, we only used

334   snow samples collected in industrial areas over northeastern China, where the light

335   absorption was dominated by fine-mode ILAPs (e.g., BC and OC; Wang et al., 2013).

336   Hence, most of the snow samples did not contain very large coarse-mode particles, such

337   as mineral and local soil dust.

338   During the snow field campaign, two series of snow samples were filtered through the

339   Nuclepore and quartz fiber filters and measured using the TSI and two-step thermal–

340   optical methods (Fig. 6). Result shows that most of the BC values measured by the TSI

341   and two-step thermal–optical methods are close to the 1:1 line in a comparison plot, and

342   are generally in good agreement (slope of 1.11, R^2 = 0.93, n = 22). However, some BC

343   values in seasonal snow measured by the two-step thermal–optical method are much

344   larger than those measured by the TSI technique. Consequently, for each sample the

mean ratio of BC concentrations measured by the two-step method and the TSI spectrophotometer varies from 0.64 to 3.97, with an overall mean of 1.57. This discrepancy arises from two factors. First, Wang et al. (2017) found that snow grain sizes varied considerably (from 0.07 to 1.3 mm) during this snow field campaign. This range is much larger than that recorded in previous studies, owing to snow melting by solar radiation and ILAPs (Hadley and Kirchstetter, 2012; Painter et al., 2013; Yasunari et al., 2013; Pedersen et al., 2015). These results agree well with those of Schwarz et al. (2012), who found that the sizes of BC particles in snow are much larger than those in typical ambient air. Therefore, the sampling efficiency of the quartz fiber filters could have been significantly higher than expected. The other factor is that the insoluble light-absorbing impurities in seasonal snow over northeast China contained not only BC, but also insoluble organic carbon. This result is consistent with a previous study by Chow et al. (2004), who reported that the charring observed when employing the two-step thermal–optical method at higher temperatures (>550°C) was incomplete and that certain organic compounds are not completely pyrolyzed below 550°C. Therefore, incomplete charring of absorbed organic compounds by the two-step processes may lead to incompletely pyrolyzed OC on the filters, artificially contributing to the BC concentration. This may explain why the BC concentration measured using the thermal–optical method was higher than that measured using the TSI spectrophotometer.

A comparison of BC concentrations in the atmosphere measured by the ISSW and thermal–optical methods is vastly different than that for the snow samples (Fig. 7). Results are in excellent agreement for BC concentrations of <3 μg m^{-3}. However, biases increased gradually with increasing BC concentrations, leading to two-step-to-TSI ratios as low as 0.5. The BC concentrations of >3 μg m^{-3} obtained using the two-step thermal–optical method are much lower than those measured using the improved TSI technique, possibly due to the small particle sizes in the atmosphere, which lead to a lower filtration efficiency. Overall, we conclude that the improved TSI method is more stable and suitable for measuring BC concentrations in both the atmosphere and snow samples compared with the two-step thermal–optical method.

374 3.3 Spatial distribution of BC and non-BC light absorption measured by the TSI

375 spectrophotometer

376   The above results show that the improved TSI method measures BC concentrations in

377   the atmosphere and snow/ice with higher accuracy than Two-step thermal optical

378   methods. In this section we investigate the spatial distribution of BC concentrations and

379   their relative light absorption due to BC and non-BC snow impurities in seasonal snow

380   over northeast China during January–February 2014. All BC mass concentrations in

381   surface snow measured by the TSI and thermal–optical methods during the snow field

382   campaigns are listed in Table 2. There was less snow fall in January 2014 than in 2010,

383   and seasonal snow did not cover all of central Inner Mongolia during this time. Thus, we

384   only collected snow samples at site 90. Given that this region is windy, the surface snow

385   collected included drifted and aged snow. The surface BC concentration was 350 ng g^{-1}

386   in the central Inner Mongolia region. The lowest BC concentrations in surface snow, 55

387   and 280 ng g^{-1}, were found on the border of northeast China (sites 91–97). We note that

388   there were considerable variations in BC concentrations in these regions. The median BC

389   concentration was 1100 ng g^{-1} with a range of 520–3900 ng g^{-1} for surface snow in

390   northeast industrial regions. On 10 February 2014, fresh snow samples were collected in

391   Lanzhou, at a mean snow depth of 6–8 cm. The mean BC concentration in these fresh

392   snow samples from Lanzhou was ~170 ng g^{-1}.

393   The relative light absorption due to BC and non-BC fractions in seasonal snow

394   measured using the improved TSI technique across northern China is shown in Figure 8.

395   A similar pattern for the light absorption of BC (~70%) and non-BC (~30%) from

396   insoluble light-absorbing impurities in surface snow indicates a similar pollution

397   emission source over northeast China. However, the light absorption due to BC in

398   seasonal snow plays a dominant role (43.11%–88.56%, with a mean of 73.10%). The

399   largest BC light absorption was at site 102. This site is located in the central part of Jilin

400   province, which is polluted by heavy industrial activity. For one sample, the light

401   absorption of non-BC impurities in seasonal snow reached 56.89%, which is the only

402   time it exceeded BC light-absorption. Biomass burning and fossil fuel are likely the

403   major emission sources during the winter in Lanzhou, unlike the case over northeast

404   China. These results are consistent with those of Wang et al. (2013), who found that snow

405   particle light absorption was dominated by BC in northeast China in 2010.

406   Finally, we investigate atmospheric BC mass concentrations and their relative light

407   absorption measured by the TSI spectrophotometer in Lanzhou during 5–25 August 2015.

408   During this experiment, there were no noticeable trends of BC concentrations in Lanzhou.

409   However, a notable feature in Figure 9 is that the BC mass concentrations at night are

410   generally much higher than during the day (Table 3). The unique topography of Lanzhou

411   likely plays an important role in this phenomenon. Lanzhou is situated in a valley basin

412   with low rainfall, high evaporation, low wind speeds, and high calm-wind frequency,

413   which often leads to a thick inversion layer in which air pollutants accumulate during the

414   night. The light absorption due to BC in the atmosphere ranges from 62.76% to 91.84%,

415   with a mean of 75.43%.

416   **4   Conclusions**

417   We developed an improved two-sphere integration (TSI) spectrophotometer to

418   quantify BC concentrations in snow and atmospheric samples over northern China. The

419   TSI technique significantly reduces scattering effects caused by insoluble impurities

420   deposited on filters. Therefore, the system more accurately measures light absorption due

421   to BC and non-BC impurities. A system calibration using theoretical calculations for

422   standard fullerene soot revealed that the TSI system can be used to assess BC

423   concentrations with low uncertainty. A laboratory comparison revealed that the thermal–

424   optical method can lead to a significant underestimate (35%–45%) of BC concentrations

425   for small-diameter particles (~50 nm) due to the low filtration efficiency of 1-μm quartz

426   fiber filters.

427   To further assess the accuracy of the improved TSI system, two field campaigns were

428   carried out to collect seasonal snow and atmospheric samples during January–February

429   2014 and 5–25 August 2015 across northern China, respectively. Although the BC

430   concentrations measured by the TSI and thermal–optical methods are well correlated for

431   both the snow and atmospheric samples, we find that some BC values in seasonal snow

432   measured by the two-step thermal–optical method were significantly overestimated

433   compared with those measured by the TSI technique, by a factor of 1.57. Overall, the

434   improved TSI optical system developed here is applicable to quantifications of BC

435   concentrations in the atmosphere and snow/ice.

436   The spatial distribution of BC concentrations in seasonal snow over northern China

437   during January–February 2014 ranged from 60 to 3800 ng g^{-1}, with a mean value of 700

438   ng g^{-1}, and ranged from 0.78 to 7.75 μg m^{-3} in the atmosphere during 5–25 August 2015

439   in Lanzhou. The spatial distribution of BC concentrations shows that large BC values are

440   found mainly in the center of industrial regions near the central part, whereas lower

441   values are found in northeast China. Light absorption is dominated by BC (~40% to 90%)

442   in seasonal snow over northeast China, and this plays a dominant role in accelerating

443   snow melt. Atmospheric samples collected in Lanzhou show significant changes in BC

444   concentrations between day and night. Frequent, stable atmospheric boundary layers at

445   night during summer, caused by the valley-basin topography of Lanzhou, are largely

446   responsible for air pollutant accumulation during the night.

447

448

449

450

463

464

465

466 **References**

467 Andreae, M.O. and Gelencser, A.: Black carbon or brown carbon? The nature of

468   light-absorbing carbonaceous aerosols, Atmos. Chem. Phys., 6, 3131-3148, doi:

469   10.5194/acp-6-3131-2006, 2006.

470 Ban-Weiss, G.A., Cao, L., Bala, G., and Caldeira, K.: Dependence of climate forcing and

471   response on the altitude of black carbon aerosols, Clim. Dyn., 38, 897-911, doi:

472   10.1007/s00382-011-1052-y, 2012.

473 Ballach, J., Hitzenberger, R., Schultz, E., and Jaeschke, W.: Development of an

474   improved optical transmission technique for black carbon (BC) analysis, Atmos.

475   Environ. , 35, 2089-2100, doi: 10.1016/S1352-2310(00)00499-4, 2001.

476 Baumgardner, D., Kok, G., and Raga, G.: Warming of the Arctic lower stratosphere by

477   light absorbing particles, Geophys. Res. Lett., 31, doi: 10.1029/2003GL018883,

478   2004.

479 Baumgardner, D., Popovicheva, O., Allan, J., Bernardoni, V., Cao, J., Cavalli, F., Cozic, J.,

480   Diapouli, E., Eleftheriadis, K., Genberg, P.J., Gonzalez, C., Gysel, M., John, A.,

481   Kirchstetter, T.W., Kuhlbusch, T.A.J., Laborde, M., Lack, D., Muller, T., Niessner, R.,

482   Petzold, A., Piazzalunga, A., Putaud, J.P., Schwarz, J., Sheridan, P., Subramanian, R.,

483   Swietlicki, E., Valli, G., Vecchi, R., and Viana, M.: Soot reference materials for

484   instrument calibration and intercomparisons: a workshop summary with

485   recommendations, Atmos. Meas. Tech., 5, 1869-1887, doi:

486   10.5194/amt-5-1869-2012, 2012.

487 Birch, M.E.: Analysis of carbonaceous aerosols: interlaboratory comparison, Analyst

488   123, 851-857, doi: 10.1039/A800028J, 1998.

489   Birch, M. E., and Cary, R. A.: Elemental carbon-based method for monitoring

490   occupational exposures to particulate diesel exhaust, Aerosol Sci. Technol., 25,

491   221-241, doi: 10.1080/02786829608965393, 1996.

492   Bond, T.C., Bussemer, M., Wehner, B., Keller, S., Charlson, R.J., and Heintzenberg, J.:

493   Light absorption by primary particle emissions from a lignite burning plant,

494   Environ. Sci. Technol., 33, 3887-3891, doi: 10.1021/es9810538, 1999.

495   Bond, T.C., Streets, D.G., Yarber, K.F., Nelson, S.M., Woo, J.H., and Klimont, Z.: A

496   technology-based global inventory of black and organic carbon emissions from

497   combustion, J. Geophys. Res.-Atmos., 109, doi:10.1029/2003JD003697, 2004.

498   Bond, T.C., Doherty, S.J., Fahey, D.W., Forster, P.M., Berntsen, T., DeAngelo, B.J.,

499   Flanner, M.G., Ghan, S., Karcher, B., Koch, D., Kinne, S., Kondo, Y., Quinn, P.K.,

500   Sarofim, M.C., Schultz, M.G., Schulz, M., Venkataraman, C., Zhang, H., Zhang, S.,

501   Bellouin, N., Guttikunda, S.K., Hopke, P.K., Jacobson, M.Z., Kaiser, J.W., Klimont, Z.,

502   Lohmann, U., Schwarz, J.P., Shindell, D., Storelvmo, T., Warren, S.G., and Zender,

503   C.S.: Bounding the role of black carbon in the climate system: A scientific

504   assessment, J. Geophys. Res.-Atmos., 118, 5380-5552, doi: 10.1002/jgrd.50171,

505   2013.

506   Cachier, H., Bremond, M.P., and Buat-Menard, P.: Determination of atmospheric soot

507   carbon with a simple thermal method, Tellus B., 41, 379-390, doi:

508   10.1111/j.1600-0889.1989.tb00316.x , 1989.

509   Cachier, H. and Pertuisot, M.H.: Particulate Carbon in Arctic Ice, Analusis, 22,

510   M34-M37, 1994.

511   Cao, J.J., Lee, S.C., Ho, K.F., Zhang, X.Y., Zou, S.C., Fung, K., Chow, J.C., and Watson, J.G.:

512   Characteristics of carbonaceous aerosol in Pearl River Delta Region, China during

513   2001 winter period, Atmos. Environ., 37, 1451-1460, doi:

514   10.1016/S1352-2310(02)01002-6, 2003.

515   Cao, J.J., Wu, F., Chow, J.C., Lee, S.C., Li, Y., Chen, S.W., An, Z.S., Fung, K.K., Watson, J.G.,

516   Zhu, C.S., and Liu, S.X.: Characterization and source apportionment of atmospheric

517   organic and elemental carbon during fall and winter of 2003 in Xi'an, China,

518   Atmos. Chem. Phys., 5, 3127-3137, doi: 10.5194/acp-5-3127-2005, 2005.

519 Cao, J.J., Lee, S.C., Chow, J.C., Watson, J.G., Ho, K.F., Zhang, R.J., Jin, Z.D., Shen, Z.X., Chen,

520   G.C., Kang, Y.M., Zou, S.C., Zhang, L.Z., Qi, S.H., Dai, M.H., Cheng, Y., and Hu, K.:

521   Spatial and seasonal distributions of carbonaceous aerosols over China, J.

522   Geophys. Res.-Atmos., 112, doi: 10.1029/2006JD008205, 2007.

523 Carmagnola, C.M., Domine, F., Dumont, M., Wright, P., Strellis, B., Bergin, M., Dibb, J.,

524   Picard, G., Libois, Q., Arnaud, L., and Morin, S.: Snow spectral albedo at Summit,

525   Greenland: measurements and numerical simulations based on physical and

526   chemical properties of the snowpack, The Cryosphere, 7, 1139-1160, doi:

527   10.5194/tc-7-1139-2013, 2013.

528 Chen, L.W.A., Chow, J.C., Watson, J.G., Moosmuller, H., and Arnott, W.P.: Modeling

529   reflectance and transmittance of quartz-fiber filter samples containing elemental

530   carbon particles: Implications for thermal/optical analysis, J. Aerosol Sci., 35,

531   765-780, doi: 10.1016/j.jaerosci.2003.12.005, 2004.

532 Chow, J.C., Watson, J.G., Pritchett, L.C., Pierson, W.R., Frazier, C.A., and Purcell, R.G.:

533   The Dri Thermal Optical Reflectance Carbon Analysis System - Description,

534   Evaluation and Applications in United-States Air-Quality Studies, Atmos. Environ.,

535   27, 1185-1201, doi: 10.1016/0960-1686(93)90245-T , 1993.

536 Chow, J.C., Watson, J.G., Lu, Z.Q., Lowenthal, D.H., Frazier, C. A., Solomon, P. A.,

537   Thuillier, R. H., Magliano, K.: Descriptive analysis of PM(2.5) and PM(10) at

538   regionally representative locations during SJVAQS/AUSPEX. Atmos. Environ., 30,

539   2079-2112, doi: 10.1016/1352-2310(95)00402-5, 1996.

540 Chow, J.C., Watson, J.G., Crow, D., Lowenthal, D.H., and Merrifield, T.: Comparison of

541   IMPROVE and NIOSH carbon measurements, Aerosol Sci. Technol., 34, 23-34, doi:

542   10.1080/02786820119073, 2001.

543 Chow, J.C., Watson, J.G., Chen, L.W.A., Arnott, W.P., Moosmuller, H., and Fung, K.:

544   Equivalence of elemental carbon by thermal/optical reflectance and

545   transmittance with different temperature protocols, Environ. Sci. Technol., 38,

546   4414-4422, doi: 10.1021/es034936u, 2004.

547 Chuang, C.C., Penner, J.E., Prospero, J.M., Grant, K.E., Rau, G.H., and Kawamoto, K.:

548   Cloud susceptibility and the first aerosol indirect forcing: Sensitivity to black

549   carbon and aerosol concentrations, J. Geophys. Res.-Atmos., 107, doi:
550   10.1029/2000JD000215, 2002.

551 Chylek, P., Srivastava, V., Cahenzli, L., Pinnick, R.G., Dod, R.L., Novakov, T., Cook, T.L.,
552   and Hinds, B.D.: Aerosol and Graphitic Carbon Content of Snow, J. Geophys.
553   Res.-Atmos., 92, 9801-9809, doi: 10.1029/JD092iD08p09801, 1987.

554 Clarke, A.D., Noone, K.J., Heintzenberg, J., Warren, S.G., and Covert, D.S.: Aerosol
555   Light-Absorption Measurement Techniques - Analysis and Intercomparisons,
556   Atmos. Environ., 21, 1455-1465, doi: 10.1016/0004-6981(67)90093-5, 1967.

557 Cong, Z., Kang, S., Kawamura, K., Liu, B., Wan, X., Wang, Z., Gao, S., and Fu, P.:
558   Carbonaceous aerosols on the south edge of the Tibetan Plateau: concentrations,
559   seasonality and sources, Atmos. Chem. Phys., 15, 1573-1584, doi:
560   10.5194/acp-15-1573-2015, 2015.

561 Cross, E.S., Onasch, T.B., Ahern, A., Wrobel, W., Slowik, J.G., Olfert, J., Lack, D.A.,
562   Massoli, P., Cappa, C.D., Schwarz, J.P., Spackman, J.R., Fahey, D.W., Sedlacek, A.,
563   Trimborn, A., Jayne, J.T., Freedman, A.,Williams, L.R., Ng, N.L., Mazzoleni, C., Dubey,
564   M., Brem, B., Kok, G., Subramanian, R., Freitag, S., Clarke, A., Thornhill, D., Marr,
565   L.C., Kolb, C.E., Worsnop, D.R., and Davidovits, P.: Soot Particle Studies-Instrument
566   Inter-Comparison-Project Overview, Aerosol Sci. Technol., 44, 592–611, 2010.

567 Dang, C. and Hegg, D.A.: Quantifying light absorption by organic carbon in Western
568   North American snow by serial chemical extractions, J. Geophys. Res.-Atmos., 119,
569   10247-10261, doi: 10.1002/2014JD022156, 2014.

570 Doherty, S.J., Warren, S.G., Grenfell, T.C., Clarke, A.D., and Brandt, R.E.:
571   Light-absorbing impurities in Arctic snow, Atmos. Chem. Phys., 10, 11647-11680,
572   doi: 10.5194/acp-10-11647-2010, 2010.

573 Doherty, S.J., Dang, C., Hegg, D.A., Zhang, R.D., and Warren, S.G.: Black carbon and
574   other light-absorbing particles in snow of central North America, J. Geophys.
575   Res.-Atmos., 119, 12807-12831, doi: 10.1002/2014JD022350, 2014.

576 Fischer K.: Bestimmung der Absorption von sichtbarer Strahlung durch
577   Aerosolpartikeln, Contr. Atmos. Phys., 43, 244-254, 1970.

578 Flanner, M.G., Liu, X., Zhou, C., Penner, J.E., and Jiao, C.: Enhanced solar energy
579   absorption by internally-mixed black carbon in snow grains, Atmos. Chem. Phys.,
580   12, 4699-4721, doi: 10.5194/acp-12-4699-2012, 2012.

581 Forsstrom, S., Isaksson, E., Skeie, R.B., Strom, J., Pedersen, C.A., Hudson, S.R.,
582   Berntsen, T.K., Lihavainen, H., Godtliebsen, and F., Gerland, S.: Elemental carbon
583   measurements in European Arctic snow packs, J. Geophys. Res.-Atmos., 118,
584   13614-13627, doi: 10.1002/2013JD019886, 2013.

585 Gillies, J. A., Gertler, A.W., Sagebiel, J.C., Dippel, W.A.: On-road particulate matter
586   (PM2.5 and PM10) emissions in the Sepulveda Tunnel, Los Angeles, California.
587   Environ. Sci. Technol., 35, 1054-1063, 2001.

588 Gray, H. A., Cass, G. R., Huntzicker, J. J., Heyerdahl, E.K., Rau, J.A.: Characteristics of
589   Atmospheric Organic and Elemental Carbon Particle Concentrations in
590   Los-Angeles. Environ. Sci. Technol., 20, 580-589, doi: 10.1021/Es00148a006,
591   1986.

592 Grenfell, T.C., Doherty, S.J., Clarke, A.D., and Warren, S.G.: Light absorption from
593   particulate impurities in snow and ice determined by spectrophotometric
594   analysis of filters, Appl. Opt., 50, 2037-2048, doi: 10.1364/AO.50.002037, 2011.

595 Hadley, O.L., Corrigan, C.E., Kirchstetter, T.W., Cliff, S.S., and Ramanathan, V.:
596   Measured black carbon deposition on the Sierra Nevada snow pack and
597   implication for snow pack retreat, Atmos. Chem. Phys., 10, 7505-7513, doi:
598   10.5194/acp-10-7505-2010, 2010.

599 Hadley, O.L. and Kirchstetter, T.W.: Black-carbon reduction of snow albedo, Nat.
600   Clim. Chang., 2, 437-440, doi: 10.1038/NCLIMATE1433, 2012.

601 Han, Y. M., Han, Z. W., Cao, J. J., Chow, J.C., Watson, J.G., An, Z.S., Liu, S.X., Zhang, R.J.:
602   Distribution and origin of carbonaceous aerosol over a rural high-mountain lake
603   area, Northern China and its transport significance. Atmos. Environ., 42,
604   2405-2414, doi: 10.1016/j.atmosenv.2007.12.020, 2008.

605 Hansen, A. D. A., Rosen, H., and Novakov, T.: The aethalometer — An instrument for
606   the real-time measurement of optical absorption by aerosol particles, Sci. Total
607   Environ., 36, 191-196, doi: 10.1016/0048-9697(84)90265-1, 1984.

608 Hansen, J., Sato, M., Ruedy, R., Nazarenko, L., Lacis, A., Schmidt, G.A., Russell, G.,
609   Aleinov, I., Bauer, M., Bauer, S., Bell, N., Cairns, B., Canuto, V., Chandler, M., Cheng,
610   Y., Del Genio, A., Faluvegi, G., Fleming, E., Friend, A., Hall, T., Jackman, C., Kelley, M.,
611   Kiang, N., Koch, D., Lean, J., Lerner, J., Lo, K., Menon, S., Miller, R., Minnis, P.,
612   Novakov, T., Oinas, V., Perlwitz, J., Perlwitz, J., Rind, D., Romanou, A., Shindell, D.,
613   Stone, P., Sun, S., Tausnev, N., Thresher, D., Wielicki, B., Wong, T., Yao, M., and
614   Zhang, S.: Efficacy of climate forcings, J. Geophys. Res.-Atmos., 110, doi:
615   10.1029/2005JD005776, 2005.

616 Heintzenberg, J.: Fine particles in the global troposphere A review, Tellus B., 41,
617   149-160, doi: 10.1111/j.1600-0889.1989.tb00132.x, 1989.

618 Hitzenberger, R.: Absorption-Measurements with an Integrating Plate Photometer
619   Calibration and Error Analysis, Aerosol Sci. Technol., 18, 70-84, doi:
620   10.1080/02786829308959585, 1993.

621 Horvath, H.: Comparison of Measurements of Aerosol Optical-Absorption by Filter
622   Collection and a Transmissometric Method, Atmos. Environ., 27, 319-325, doi:
623   10.1016/0960-1686(93)90105-8, 1993a.

624 Horvath, H.: Atmospheric Light-Absorption - a Review, Atmos. Environ., 27, 293-317,
625   doi: 10.1016/0960-1686(93)90104-7, 1993b.

626 Huang, J.P., Fu, Q.A., Zhang, W., Wang, X., Zhang, R.D., Ye, H., and Warren, S.G.: Dust
627   and Black Carbon in Seasonal Snow across Northern China, Bull. Amer. Meteor.
628   Soc., 92, 175-181, doi: 10.1175/2010BAMS3064.1, 2011.

629 IPCC. 2013. Climate Change 2013: The Physical Science Basis[M]. Stocker, T. F., D .
630   Qin, G. K. Plattner, et al., Cambridge, United Kingdom and New York, NY, USA.

631 Ivleva, N. P., McKeon, U., Niessner, R., and Pöschl, U.: Raman microspectroscopic
632   analysis of size-resolved atmospheric aerosol particle samples collected with an
633   ELPI: Soot, humic-like substances, and inorganic compounds, Aerosol Sci.
634   Technol., 41, 655–671, doi:10.1080/02786820701376391, 2007.

635 Jacobson, M.Z.: Strong radiative heating due to the mixing state of black carbon in
636   atmospheric aerosols, Nature 409, 695-697, doi: 10.1038/35055518, 2001a.

637   Jacobson, M.Z.: Global direct radiative forcing due to multicomponent anthropogenic

638   and natural aerosols, J. Geophys. Res.-Atmos., 106, 1551-1568, doi:

639   10.1029/2000JD900514, 2001b.

640   Jenk, T.M., Szidat, S., Schwikowski, M., Gaggeler, H.W., Brutsch, S., Wacker, L., Synal,

641   H.A., and Saurer, M.: Radiocarbon analysis in an Alpine ice core: record of

642   anthropogenic and biogenic contributions to carbonaceous aerosols in the past

643   (1650-1940), Atmos. Chem. Phys., 6, 5381-5390, doi: 10.5194/acp-6-5381-2006,

644   2006.

645   Jimenez, J. L., Canagaratna, M. R., Donahue, N. M., Prevot, A.S.H., Zhang, Q., Kroll, J.H.,

646   DeCarlo, P.F., Allan, J.D., Coe, H., Ng, N.L., Aiken, A.C., Docherty, K.S., Ulbrich, I.M.,

647   Grieshop, A.P., Robinson, A.L., Duplissy, J., Smith, J.D., Wilson, K.R., Lanz, V.A.,

648   Hueglin, C., Sun, Y.L., Tian, J., Laaksonen, A., Raatikainen, T., Rautiainen, J.,

649   Vaattovaara, P., Ehn, M., Kulmala, M., Tomlinson, J.M., Collins, D.R., Cubison, M.J.,

650   Dunlea, E.J., Huffman, J.A., Onasch, T.B., Alfarra, M.R., Williams, P.I., Bower, K.,

651   Kondo, Y., Schneider, J., Drewnick, F., Borrmann, S., Weimer, S., Demerjian, K.,

652   Salcedo, D., Cottrell, L., Griffin, R., Takami, A., Miyoshi, T., Hatakeyama, S., Shimono,

653   A., Sun, J.Y., Zhang, Y.M., Dzepina, K., Kimmel, J.R., Sueper, D., Jayne, J.T., Herndon,

654   S.C., Trimborn, A.M., Williams, L.R., Wood, E.C., Middlebrook, A.M., Kolb, C.E.,

655   Baltensperger, U., Worsnop, D.R.: Evolution of organic aerosols in the atmosphere,

656   Science, 326, 1525–1529, 2009.

657   Koch, D., Schulz, M., Kinne, S., McNaughton, C., Spackman, J.R., Balkanski, Y., Bauer, S.,

658   Berntsen, T., Bond, T.C., Boucher, O., Chin, M., Clarke, A., De Luca, N., Dentener, F.,

659   Diehl, T., Dubovik, O., Easter, R., Fahey, D.W., Feichter, J., Fillmore, D., Freitag, S.,

660   Ghan, S., Ginoux, P., Gong, S., Horowitz, L., Iversen, T., Kirkevag, A., Klimont, Z.,

661   Kondo, Y., Krol, M., Liu, X., Miller, R., Montanaro, V., Moteki, N., Myhre, G., Penner,

662   J.E., Perlwitz, J., Pitari, G., Reddy, S., Sahu, L., Sakamoto, H., Schuster, G., Schwarz,

663   J.P., Seland, O., Stier, P., Takegawa, N., Takemura, T., Textor, C., van Aardenne, J.A.,

664   and Zhao, Y.: Evaluation of black carbon estimations in global aerosol models,

665   Atmos. Chem. Phys., 9, 9001-9026, doi: 10.5194/acp-9-9001-2009, 2009.

666 Legrand, M., Preunkert, S., Schock, M., Cerqueira, M., Kasper-Giebl, A., Afonso, J., Pio,
667   C., Gelencser, A., and Dombrowski-Etchevers, I.: Major 20th century changes of
668   carbonaceous aerosol components (EC, WinOC, DOC, HULIS, carboxylic acids, and
669   cellulose) derived from Alpine ice cores, J. Geophys. Res.-Atmos., 112, doi:
670   10.1029/2006JD008080, 2007.

671 Li, W., Shao, L., Zhang, D., Ro, C.-U., Hu, M., Bi, X., Geng, H., Matsuki, A., Niu, H., and
672   Chen, J.: A review of single aerosol particle studies in the atmosphere of East Asia:
673   morphology, mixing state, source, and heterogeneous reactions, J. Clean Prod.,
674   112, 1330-1349, https://doi.org/10.1016/j.jclepro.2015.04.050, 2016.

675 Lim, S., Fain, X., Zanatta, M., Cozic, J., Jaffrezo, J.L., Ginot, P., and Laj, P.: Refractory
676   black carbon mass concentrations in snow and ice: method evaluation and
677   inter-comparison with elemental carbon measurement, Atmos. Meas. Tech., 7,
678   3307-3324, doi: 10.5194/amt-7-3307-2014, 2014.

679 McMeeking, G.R., Morgan, W.T., Flynn, M., Highwood, E.J., Turnbull, K., Haywood, J.,
680   and Coe, H.: Black carbon aerosol mixing state, organic aerosols and aerosol
681   optical properties over the United Kingdom, Atmos. Chem. Phys., 11, 9037-9052,
682   doi: 10.5194/acp-11-9037-2011, 2011.

683 Menon, S., Hansen, J., Nazarenko, L., Luo, Y.F.: Climate effects of black carbon
684   aerosols in China and India, Science 297, 2250-2253, doi:
685   10.1126/science.1075159, 2002.

686 Ming, J., Cachier, H., Xiao, C., Qin, D., Kang, S., Hou, S., and Xu, J.: Black carbon record
687   based on a shallow Himalayan ice core and its climatic implications, Atmos. Chem.
688   Phys., 8, 1343-1352, doi: 10.5194/acp-8-1343-2008, 2008.

689 Ming, J., Xiao, C.D., Cachier, H., Qin, D.H., Qin, X., Li, Z.Q., and Pu, J.C.: Black Carbon (BC)
690   in the snow of glaciers in west China and its potential effects on albedos, Atmos.
691   Res., 92, 114-123, doi: 10.1016/j.atmosres.2008.09.007, 2009.

692 Ming, J., Xiao, C.D., Sun, J.Y., Kang, S.C., and Bonasoni, P.: Carbonaceous particles in
693   the atmosphere and precipitation of the Nam Co region, central Tibet, J. Environ.
694   Sci., 22, 1748-1756, doi: 10.1016/S1001-0742(09)60315-6, 2010.

695 Moosmuller, H., Chakrabarty, R.K., and Arnott, W.P.: Aerosol light absorption and its
696   measurement: A review, J. Quant. Spectrosc. Ra., 110, 844-878, doi:
697   10.1016/j.jqsrt.2009.02.035, 2009.

698 Moteki, N., Kondo, Y., Takegawa, N., and Nakamura, S.-i.: Directional dependence of
699   thermal emission from nonspherical carbon particles, J. Aerosol Sci., 40, 790-801,
700   doi: 10.1016/j.jaerosci.2009.05.003, 2009.

701 Murphy, D. M., Cziczo, D. J., Froyd, K. D., Hudson, P. K., Matthew, B. M., Middlebrook,
702   A. M., Peltier, R. E., Sullivan, A., Thomson, D. S., Weber, R. J.: Single-particle mass
703   spectrometry of tropospheric aerosol particles. J. Geophys. Res., 111, D23S32,
704   doi:10.1029/2006JD007340, , 2006.

705 Ogren, J. A. and Charlson, R. J.: Elemental carbon in the atmosphere– cycle and
706   lifetime, Tellus, 35B, 241–254, 1983.

707 Painter, T.H., Seidel, F.C., Bryant, A.C., Skiles, S.M., and Rittger, K.: Imaging
708   spectroscopy of albedo and radiative forcing by light-absorbing impurities in
709   mountain snow, J. Geophys. Res.-Atmos., 118, 9511-9523, doi:
710   10.1002/jgrd.50520, 2013.

711 Pan, Y.P., Wang, Y.S., Xin, J.Y., Tang, G.Q., Song, T., Wang, Y.H., Li, X.R., and Wu, F.K.:
712   Study on dissolved organic carbon in precipitation in Northern China, Atmos.
713   Environ., 44, 2350-2357, doi: 10.1016/j.atmosenv.2010.03.033, 2010.

714 Pavese, G., Calvello, M., and Esposito, F.: Black Carbon and Organic Components in
715   the Atmosphere of Southern Italy: Comparing Emissions from Different Sources
716   and Production Processes of Carbonaceous Particles, Aerosol Air Qual. Res., 12,
717   1146-1156, doi: 10.4209/aaqr.2011.12.0236, 2012.

718 Pedersen, C.A., Gallet, J.C., Strom, J., Gerland, S., Hudson, S.R., Forsstrom, S., Isaksson,
719   E., and Berntsen, T. K.: In situ observations of black carbon in snow and the
720   corresponding spectral surface albedo reduction, J. Geophys. Res.-Atmos., 120,
721   1476-1489, doi: 10.1002/2014jd022407, 2015.

722 Petzold, A., Kopp, C., and Niessner, R.: The dependence of the specific attenuation
723   cross-section on black carbon mass fraction and particle size, Atmos. Environ., 31,
724   661-672, doi: 10.1016/S1352-2310(96)00245-2, 1997.

725 Petzold, A., Ogren, J. A., Fiebig, M., Laj, P., Li, S.-M., Baltensperger, U., Holzer-Popp, T.,

726   Kinne, S., Pappalardo, G., Sugimoto, N., Wehrli, C., Wiedensohler, A., and Zhang,

727   X.-Y.: Recommendations for reporting "black carbon" measurements, Atmos.

728   Chem. Phys., 13, 8365-8379, https://doi.org/10.5194/acp-13-8365-2013, 2013.

729 Qian, Y., Wang, H., Zhang, R., Flanner, M.G., and Rasch, P.J.: A sensitivity study on

730   modeling black carbon in snow and its radiative forcing over the Arctic and

731   Northern China, Environ. Res. Lett., 9, 064001, doi:

732   10.1088/1748-9326/9/6/064001, 2014.

733 Quinn, P. K. and Bates, T. S.: North American, Asian, and Indian haze: Similar

734   regional impacts on climate? Geophys. Res. Lett., 30, 1555,

735   doi:10.1029/2003GL016934, 2003.

736 Ramanathan, V., and Carmichael, G.: Global and regional climate changes due to

737   black carbon, Nat. Geosci. , 1, 221-227, Doi 10.1038/Ngeo156, 2008.

738 Rosenfeld, D., Lohmann, U., Raga, G.B., O'Dowd, C.D., Kulmala, M., Fuzzi, S., Reissell, A.,

739   and Andreae, M.O.: Flood or drought: How do aerosols affect precipitation?

740   Science 321, 1309-1313, doi: 10.1126/science.1160606, 2008.

741 Schmid, H., Laskus, L., Abraham, H.J., Baltensperger, U., Lavanchy, V., Bizjak, M.,

742   Burba, P., Cachier, H., Crow, D., Chow, J., Gnauk, T., Even, A., ten Brink, H.M., Giesen,

743   K.P., Hitzenberger, R., Hueglin, C., Maenhaut, W., Pio, C., Carvalho, A., Putaud, J.P.,

744   Toom-Sauntry, D., and Puxbaum, H.: Results of the "carbon conference"

745   international aerosol carbon round robin test stage I, Atmos. Environ., 35,

746   2111-2121, doi: 10.1016/S1352-2310(00)00493-3, 2001.

747 Schwarz, J.P., Doherty, S.J., Li, F., Ruggiero, S.T., Tanner, C.E., Perring, A.E., Gao, R.S.,

748   and Fahey, D.W.: Assessing Single Particle Soot Photometer and Integrating

749   Sphere/Integrating Sandwich Spectrophotometer measurement techniques for

750   quantifying black carbon concentration in snow, Atmos. Meas. Tech., 5,

751   2581-2592, doi: 10.5194/amt-5-2581-2012, 2012.

752 Sharma, S., Brook, J.R., Cachier, H., Chow, J., Gaudenzi, A., and Lu, G.: Light absorption

753   and thermal measurements of black carbon in different regions of Canada, J.

754   Geophys. Res.-Atmos., 107, doi: 10.1029/2002JD002496, 2002.

755 Slater, J.F., Currie, L.A., Dibb, J.E., and Benner, B.A.: Distinguishing the relative
756   contribution of fossil fuel and biomass combustion aerosols deposited at Summit,
757   Greenland through isotopic and molecular characterization of insoluble carbon,
758   Atmos. Environ., 36, 4463-4477, doi: 10.1016/S1352-2310(02)00402-8, 2002.

759 Spencer, M.T., Shields, L.G., and Prather, K. A.: Simultaneous measurement of the
760   effective density and chemical composition of ambient aerosol particles, Environ.
761   Sci. Technol., 41, 1303–1309, doi:10.1021/es061425+, 2007.

762 Thevenon, F., Anselmetti, F.S., Bernasconi, S.M., and Schwikowski, M.: Mineral dust
763   and elemental black carbon records from an Alpine ice core (Colle Gnifetti glacier)
764   over the last millennium, J. Geophys. Res.-Atmos., 114, doi:
765   10.1029/2008JD011490, 2009.

766 Turpin, B. J., Cary, R. A., and Huntzicker, J. J.: An insitu,time-resolved analyzer for
767   aerosol organic and elemental carbon. Aerosol Sci. Technol., 12, 161-171, doi:
768   10.1080/02786829008959336, 1990.

769 Turpin, B. J., and Huntzicker, J. J.: Secondary formation of organic aerosol in the Los
770   Angeles Basin: A descriptive analysis of organic and elemental carbon
771   concentrations. Atmos. Environ., 25A, 207-215, 1991.

772 von Schneidemesser, E., Schauer, J.J., Hagler, G.S.W., and Bergin, M.H.:
773   Concentrations and sources of carbonaceous aerosol in the atmosphere of Summit,
774   Greenland, Atmos. Environ., 43, 4155-4162, doi: 10.1016/j.atmosenv.2009.05.043,
775   2009.

776 Wang, M., Xu, B., Zhao, H., Cao, J., Joswiak, D., Wu, G., and Lin, S.: The Influence of
777   Dust on Quantitative Measurements of Black Carbon in Ice and Snow when Using
778   a Thermal Optical Method, Aerosol Sci. Technol., 46, 60-69, doi:
779   10.1080/02786826.2011.605815, 2012.

780 Wang, X., Doherty, S.J., and Huang, J.P.: Black carbon and other light-absorbing
781   impurities in snow across Northern China, J. Geophys. Res.-Atmos., 118,
782   1471-1492, doi: 10.1029/2012JD018291, 2013.

783 Wang, X., Pu, W., Ren, Y., Zhang, X.L., Zhang, X.Y., Shi, J.S., Jin, H.C., Dai, M.K., Chen, Q.L.:
784   Observations and model simulations of snow albedo reduction in seasonal snow

785   due to insoluble light-absorbing particles during 2014 Chinese survey, Atmos.

786   Chem. Phys., 17, 2279-2296, doi: 10.5194/acp-17-2279-2017, 2017.

787   Wang, R, Tao, S., Balkanski, Y., Ciais, P., Boucher, O., Liu, J.F., Piao, S.L., Shen, H.Z.,

788   Vuolo, M.R., Valari, M., Chen, H., Chen, Y.C., Cozic, A., Huang, Y., Li, B.A., Li, W., Shen,

789   G.F., Wang, B., Zhang, Y.Y.: Exposure to ambient black carbon derived from a

790   unique inventory and high-resolution model. Proc. Natl. Acad. Sci. USA., 111,

791   2459-2461, doi: 10.1073/pnas.1318763111, 2014.

792   Watson, J. G., and Chow, J. C.: Comparison and evaluation of in situ and filter carbon

793   measurements at the Fresno Supersite, J. Geophys. Res.-Atmos., 107,

794   doi:10.1029/2001jd000573, 2002.

795   Wolff, E.W. and Cachier, H.: Concentrations and seasonal cycle of black carbon in

796   aerosol at a coastal Antarctic station, J. Geophys. Res.-Atmos., 103, 11033-11041,

797   doi: 10.1029/97JD01363, 1998.

798   Xu, B.Q., Yao, T.D., Liu, X.Q., and Wang, N.L.: Elemental and organic carbon

799   measurements with a two-step heating-gas chromatography system in snow

800   samples from the Tibetan Plateau, Annals of Glaciology, Vol 43, 2006 43, 257-262,

801   doi: 10.3189/172756406781812122, 2006.

802   Xu, B.Q., Cao, J.J., Hansen, J., Yao, T.D., Joswia, D.R., Wang, N.L., Wu, G.J., Wang, M.,

803   Zhao, H.B., Yang, W., Liu, X.Q., and He, J.Q.: Black soot and the survival of Tibetan

804   glaciers, Proc. Nat. Acad. Sci. U.S.A., 106, 22114-22118, doi:

805   10.1073/pnas.0910444106, 2009a.

806   Xu, B.Q., Wang, M., Joswiak, D.R., Cao, J.J., Yao, T.D., Wu, G.J., Yang, W., and Zhao, H.B.:

807   Deposition of anthropogenic aerosols in a southeastern Tibetan glacier, J. Geophys.

808   Res.-Atmos., 114, doi: 10.1029/2008JD011510, 2009b.

809   Xu, B.Q., Cao, J.J., Joswiak, D.R., Liu, X.Q., Zhao, H.B., and He, J.Q.: Post-depositional

810   enrichment of black soot in snow-pack and accelerated melting of Tibetan glaciers,

811   Environ. Res. Lett., 7, doi: 10.1088/1748-9326/7/1/014022, 2012.

812   Yang, H., and Yu, J.Z.: Uncertainties in charring correction in the analysis of

813   elemental and organic carbon in atmospheric particles by thermal/optical

814   methods, Environ. Sci. Technol., 36, 5199-5204, doi: 10.1021/es025672z , 2002.

815 Yasunari, T. J., Tan, Q., Lau, K. M., Bonasoni, P., Marinoni, A., Laj, P., Menegoz, M.,

816   Takemura, T., and Chin, M.: Estimated range of black carbon dry deposition and

817   the related snow albedo reduction over Himalayan glaciers during dry

818   pre-monsoon periods, Atmos. Environ., 78, 259-267,

819   doi:10.1016/j.atmosenv.2012.03.031, 2013.

820 Yasunari, T. J., Koster, R. D., Lau, W. K. M., Kim, K.: Impact of snow darkening via dust,

821   black carbon, and organic carbon on boreal spring climate in the Earth system. J.

822   Geophys. Res.-Atmos., 120, 5485-5503, doi: 10.1002/2014jd022977, 2015.

823 Ye, H., Zhang, R.D., Shi, J.S., Huang, J.P., Warren, S.G., and Fu, Q.: Black carbon in

824   seasonal snow across northern Xinjiang in northwestern China, Environ. Res. Lett.,

825   7, doi: 10.1088/1748-9326/7/4/044002, 2012.

826 Zhang, R.J., Ho, K.F., Cao, J.J., Han, Z.W., Zhang, M.G., Cheng, Y., and Lee, S.C.: Organic

827   carbon and elemental carbon associated with PM10 in Beijing during spring time,

828   J. Hazard. Mater., 172, 970-977, doi: 10.1016/j.jhazmat.2009.07.087, 2009.

829 Zhao, C., Hu, Z., Qian, Y., Leung, L.R., Huang, J., Huang, M., Jin, J., Flanner, M.G., Zhang,

830   R., Wang, H., Yan, H., Lu, Z., and Streets, D.G.: Simulating black carbon and dust and

831   their radiative forcing in seasonal snow: a case study over North China with field

832   campaign measurements, Atmos. Chem. Phys., 14, 11475-11491, doi:

833   10.5194/acp-14-11475-2014, 2014

834 Zhou, Y., Wang, X., Wu, X.Q., Cong, Z.Y., Wu, G.M., Ji, M.X.: Quantifying Light

835   Absorption of Iron Oxides and Carbonaceous Aerosol in Seasonal Snow across

836   Northern China, Atmosphere-Basel, 8, doi: 10.3390/atmos8040063, 2017.

837

838

839 **Figure captions:**

840 Figure 1 Sampling locations. Sites 90–102 are located in northeast China and were used for snow

841 sample collection during Jan–Feb. 2014. Snow sampling site 103 is located in Lanzhou in northwest

842 China, and was used for atmospheric sample collection during 5–25 August 2015. Sites are numbered

843 according to Wang et al. (2013) and Ye et al. (2012).

844 Figure 2 Schematic diagram of the improved two-sphere integrating spectrophotometer.

845 Figure 3 Calibration curve for standard fullerene soot at a wavelength of 550 nm. The solid line is a

846 best-fit curve for the filter measurements. S_0 and S are the detected signals for the blank and sample

847 filters, respectively, and $-\ln(S/S_0)$ is the relative attenuation.

848 Figure 4 Comparison of the theoretical and measured BC mass determined by the TSI and two-step

849 techniques in the laboratory. The solid and dot–dashed lines represent best-fit lines for the TSI and

850 two-step techniques, respectively. The dashed line is a 1:1 line.

851 Figure 5 Mass loss of standard fullerene soot on 1.0-μm quartz fiber filters determined by refiltration

852 using 0.4-μm Nuclepore filters.

853 Figure 6 Comparison of BC concentrations in snow samples over northeast China during January–

854 February 2014 determined by the TSI and two-step thermal optical methods. A 1:1 line (dashed) and a

855 linear regression fit passing through the origin (solid curve) are also shown.

856 Figure 7 As for Fig. 6, but for atmospheric samples collected at Lanzhou in northwest China during 5–

857 25 August 2015.

858 Figure 8 Spatial distributions of light absorption at 550 nm due to BC and non-BC fractions in surface

859 snow across northern China during January–February 2014.

860   Figure 9 Variations in 8-hour (a) BC concentration and (b) BC and non-BC light absorption measured

861   by TSI spectrophotometer at 550 nm at Lanzhou during 5–25 August 2015 (day: 9 am to 5 pm; night:

862   11 pm to 7 am).

863
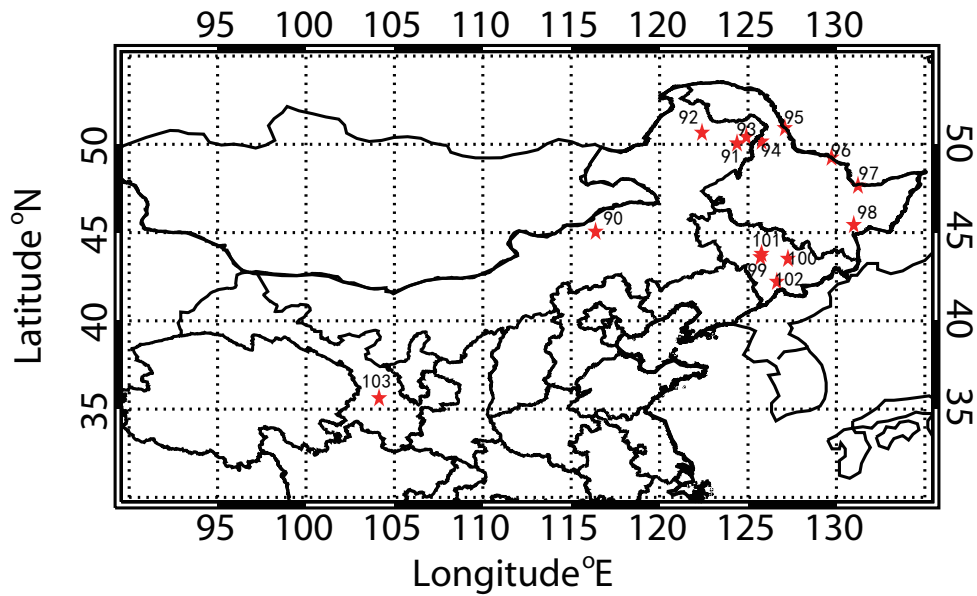
864

Figure 1 Sampling locations. Sites 90–102 are located in northeast China and were used for snow sample collection during Jan–Feb. 2014. Snow sampling site 103 is located in Lanzhou in northwest China, and was used for atmospheric sample collection during 5–25 August 2015. Sites are numbered according to Wang et al. (2013) and Ye et al. (2012).

869

870 **Table 1** Series of 15 standard filters loaded with fullerene soot, and a comparison of BC

871 concentrations between theoretical calculations and the TSI/two-step thermal–optical

872 methods in the laboratory.

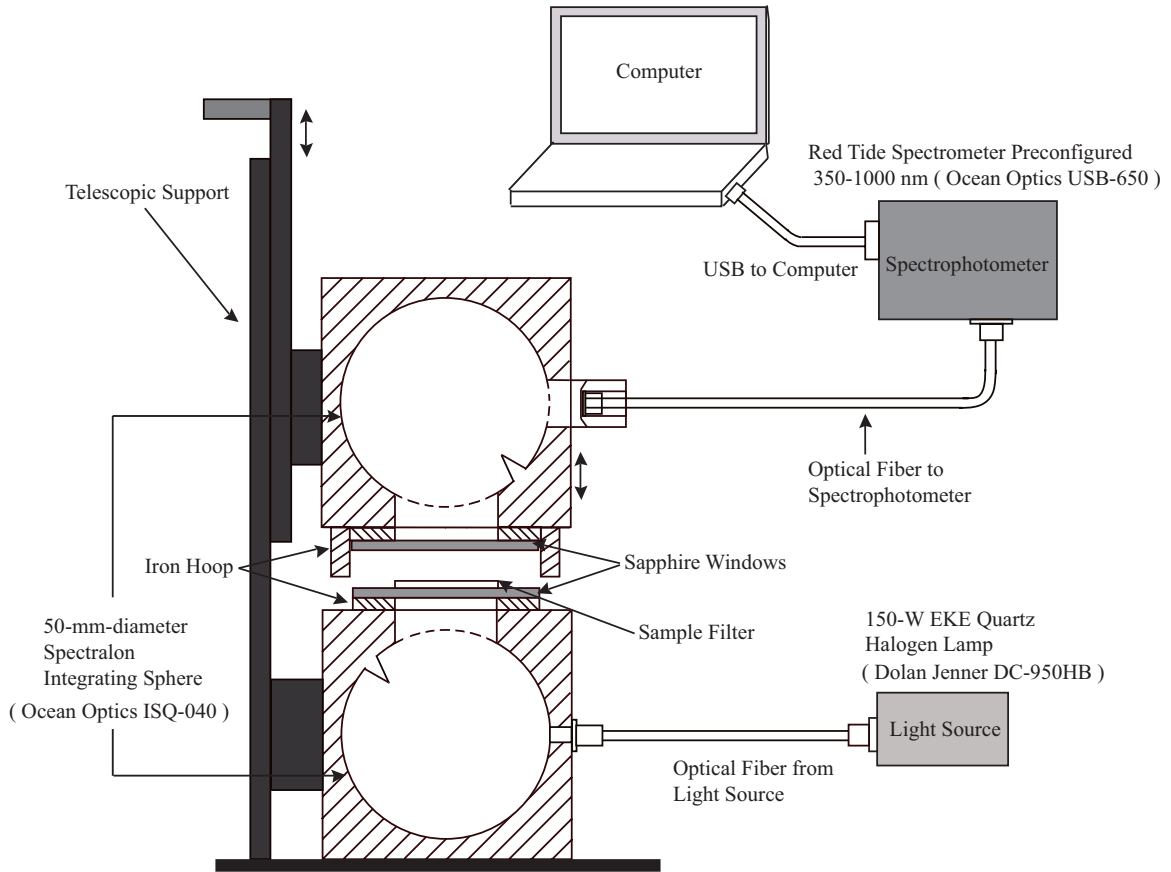| Filter	Standard BC Concentration (μg/cm^2)	Filter	Standard BC Concentration (μg/cm^2)	Filter	Calculated BC (μg)	TSI BC (μg)	Two-step BC (μg)
1	0.63	9	2.82	1	3.68	3.92	2.28
2	0.70	10	3.65	2	10.58	11.39	5.86
3	0.78	11	5.53	3	17.48	17.49	11.39
4	0.86	12	6.35	4	24.38	24.94	15.67
5	0.93	13	12.5	5	31.28	32.52	18.07
6	1.33	14	19.00	6	38.18	39.14	24.29
7	2.12	15	38.6	7	45.08	49.18	28.61
8	2.49	-	-	-	-	-	

873

874

875

876

877

878

Figure 2 Schematic diagram of the improved two-sphere integrating spectrophotometer.
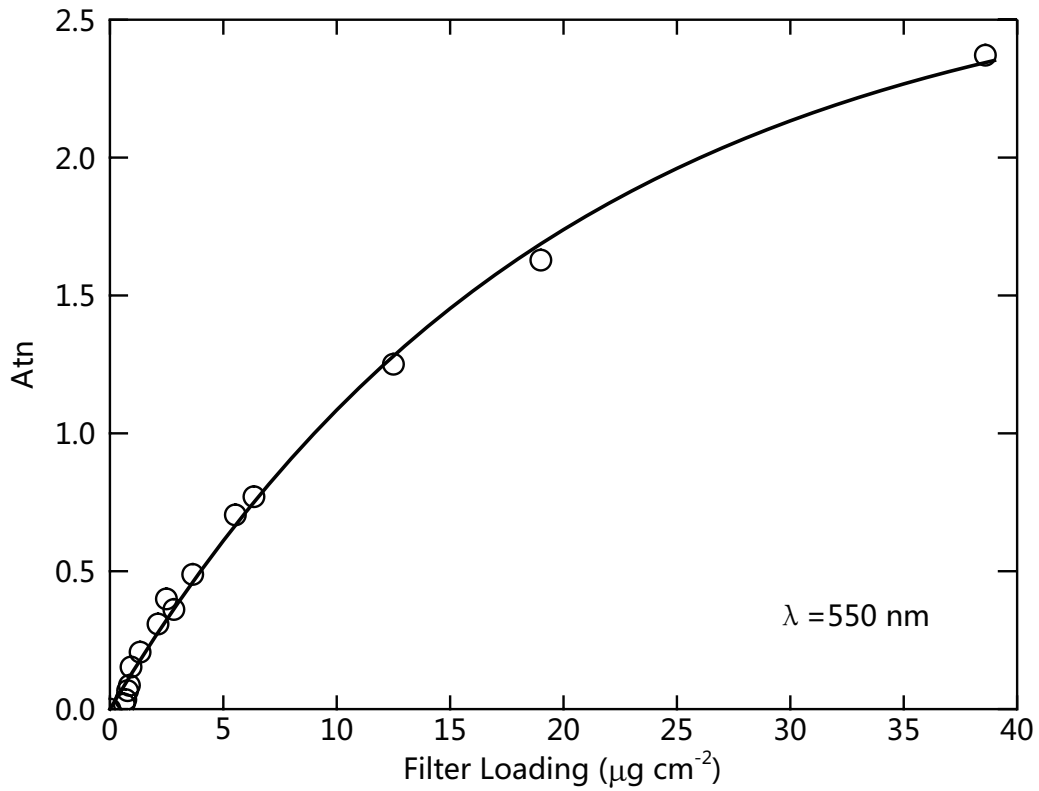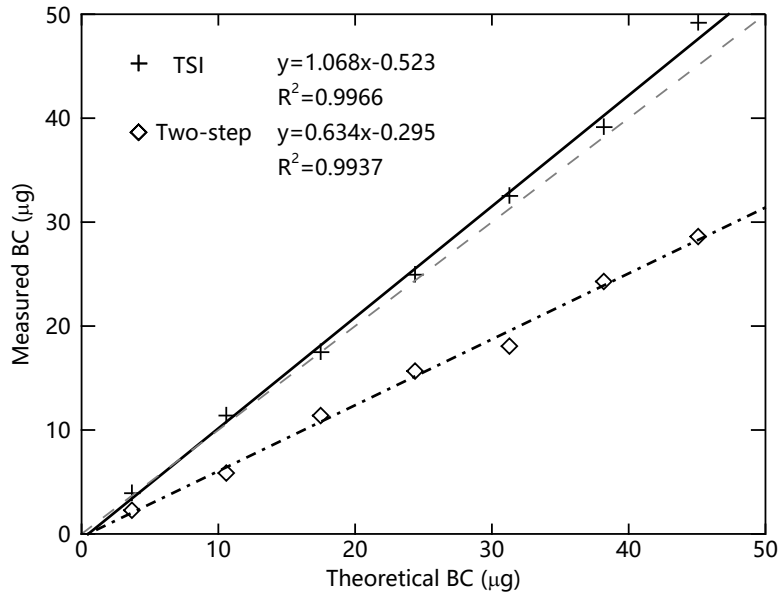
881

882

883

884

885

886

887

888

889

890

891

892

Figure 3 Calibration curve for standard fullerene soot at a wavelength of 550 nm. The solid line is a best-fit curve for the filter measurements. S_0 and S are the detected signals for the blank and sample filters, respectively, and $-\ln(S/S_0)$ is the relative attenuation.

896

897

898

899

900

901

902

903

Figure 4 Comparison of the theoretical and measured BC mass determined by the TSI and two-step techniques in the laboratory. The solid and dot–dashed lines represent best-fit lines for the TSI and two-step techniques, respectively. The dashed line is a 1:1 line.
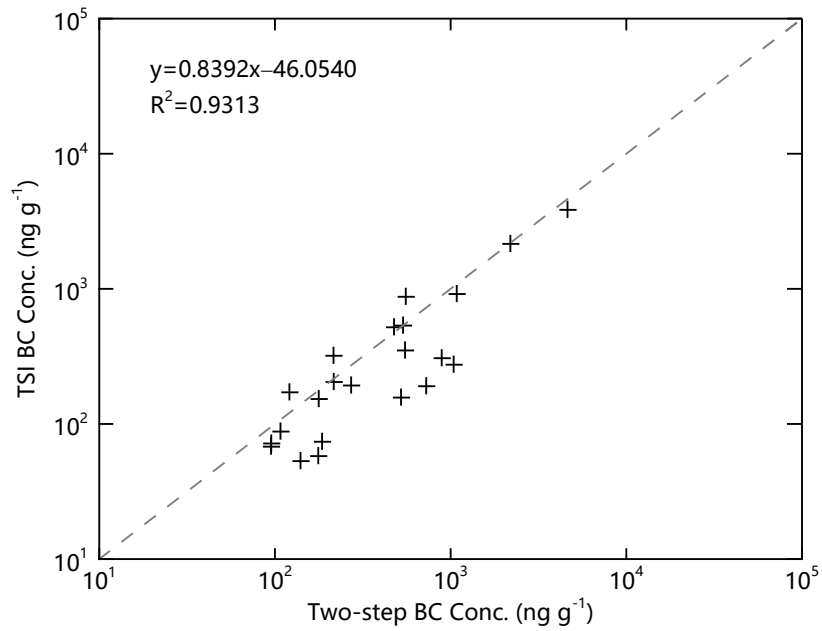
908

909

910

911

912

913

914
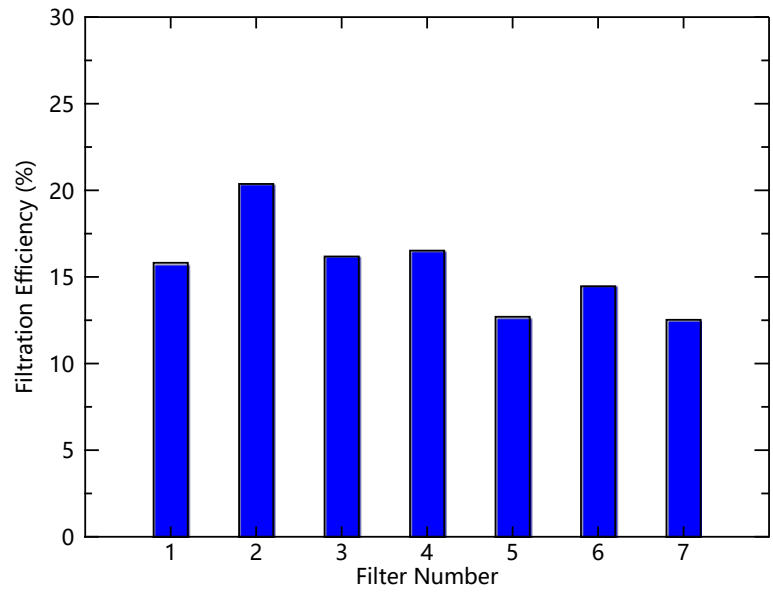
915

Figure 5 Mass loss of standard fullerene soot on 1.0-μm quartz fiber filters determined
by refiltration using 0.4-μm Nuclepore filters.

918

919

920

921

y=0.8392x−46.0540
R^2=0.9313

TSI BC Conc. (ng g^{-1})

Two-step BC Conc. (ng g^{-1})

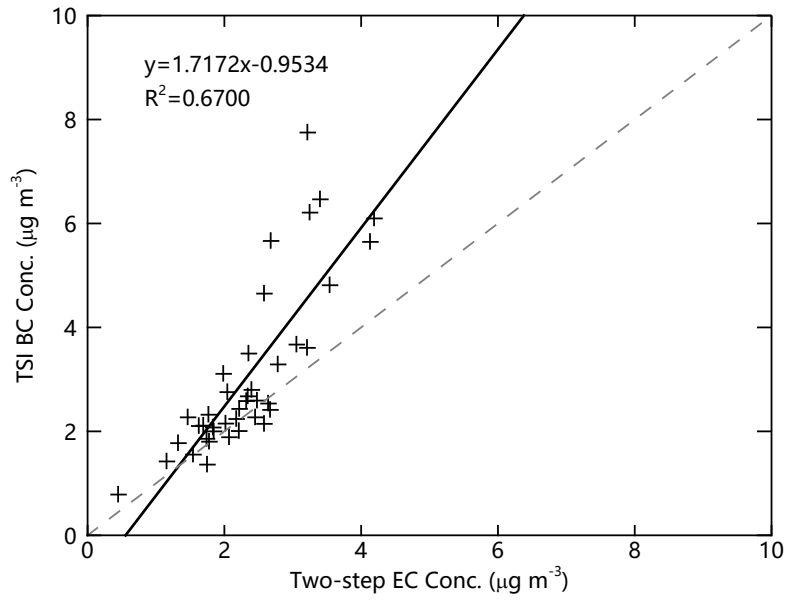922

Figure 6 Comparison of BC concentrations in snow samples over northeast China during January–February 2014 determined by the TSI and two-step thermal optical methods. A 1:1 line (dashed) and a linear regression fit passing through the origin (solid curve) are also shown.

927

928

929

930

931

932

933

Figure 7 As for Fig. 6, but for atmospheric samples collected at Lanzhou in northwest
China during 5–25 August 2015.

936

937 **Table 2** Statistics of BC and EC concentrations measured using the TSI and two-step

938 thermal–optical methods for snow samples during the experiments over northern China.

939

Site	Filter	TSI BC	Two-step EC
		ng g^{-1}	ng g^{-1}
90	Q–351L	349.95	550.19
91	Q–352L	171.46	120.87
	Q–352R	152.94	177.48
92	Q–354L	53.10	139.78
	Q–354R	57.82	176.41
93	Q–356L	71.71	95.27
	Q–356R	73.85	185.45
94	Q–358L	274.62	1040.20
95	Q–359L	87.84	107.51
	Q–359R	67.92	95.01
96	Q–363L	319.71	215.42
	Q–363R	192.60	271.42
97	Q–366L	204.47	216.04
	Q–366R	306.75	889.54
98	Q–369L	1605.95	130.36
	Q–369R	1321.69	6004.33
99	Q–376L	873.58	555.39
	Q–376R	534.70	536.11
100	Q–380R	519.47	476.14
101	Q–384R	3843.15	4626.72
102	Q–388L	915.59	1083.24
	Q–388R	2151.18	2187.90
103	Q–397L	156.76	522.07
	Q–397R	190.24	726.08

940

941
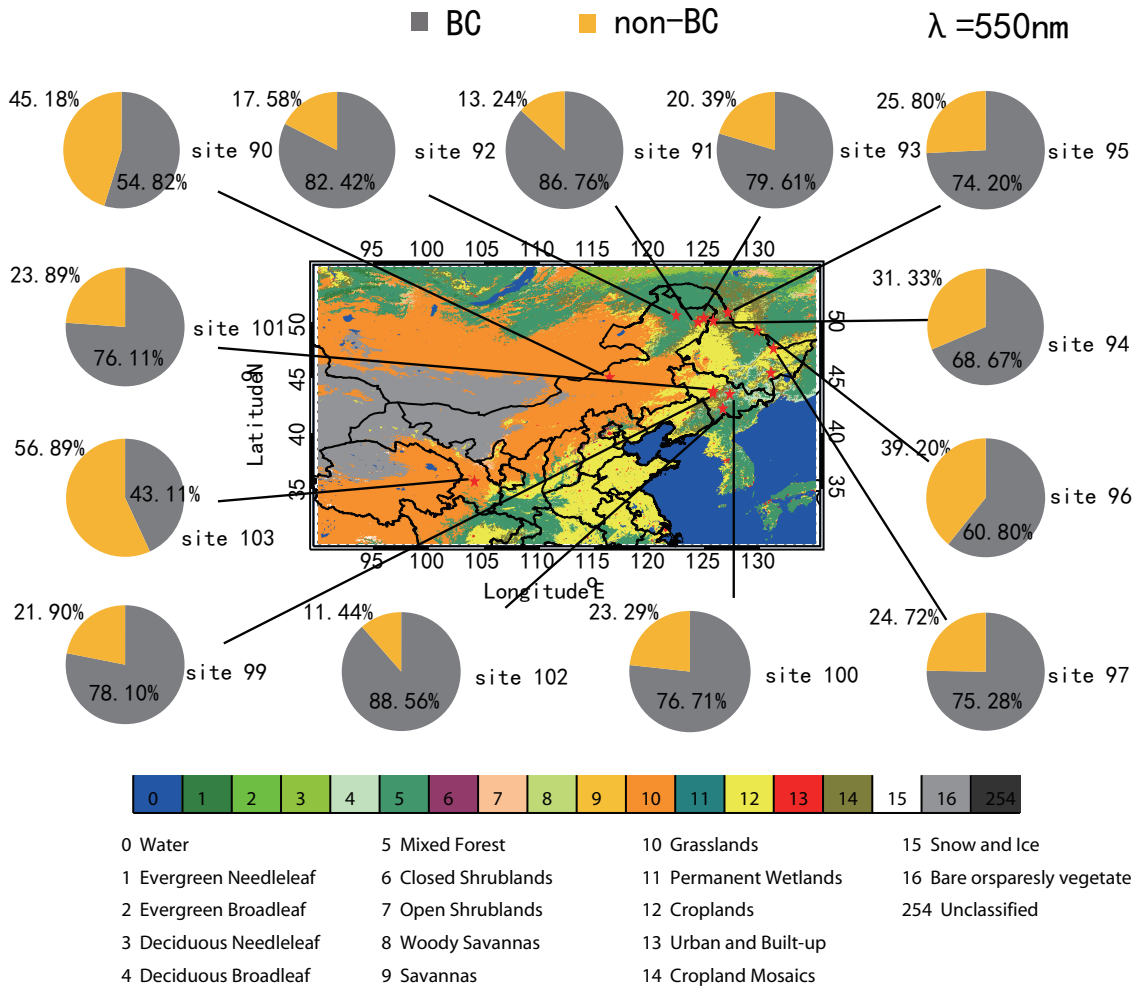
Figure 8 Spatial distributions of light absorption at 550 nm due to BC and non-BC fractions in surface snow across northern China during January–February 2014.

946
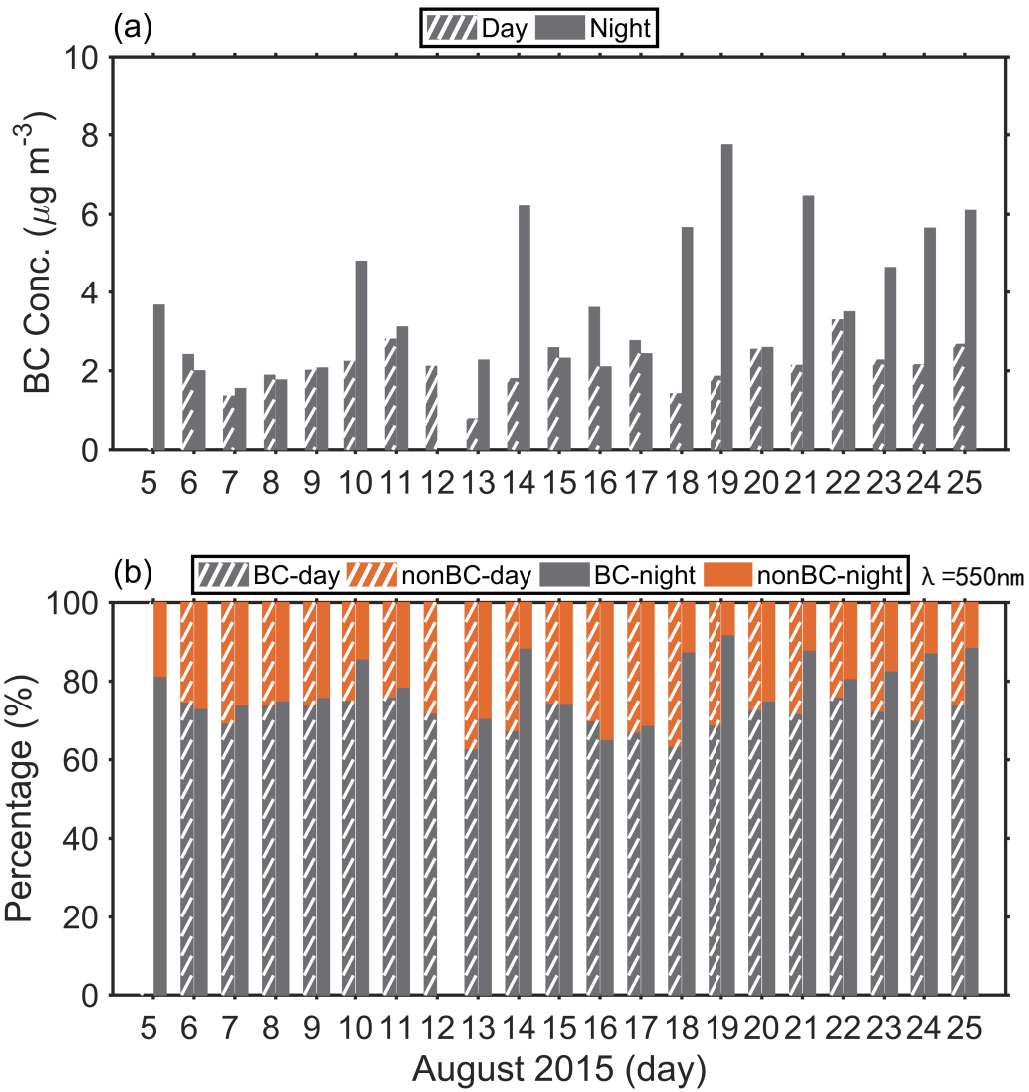
949 **Figure 9** Variations in 8-hour **(a)** BC concentration and **(b)** BC and non-BC light
950 absorption measured by TSI spectrophotometer at 550 nm at Lanzhou during 5–25
951 August 2015 (day: 9 am to 5 pm; night: 11 pm to 7 am).

952

953

954   **Table 3** Statistics of BC and EC concentrations in atmospheric samples measured using

955   the TSI and two-step thermal–optical methods.

	Day			Night		
Date	TSI BC	Two-step EC	Date	TSI BC	Two-step EC	
	$\mu g\ m^{-3}$	$\mu g\ m^{-3}$		$\mu g\ m^{-3}$	$\mu g\ m^{-3}$	
2015. 8. 6	2. 41	2. 67	2015. 8. 5–8. 6	3. 67	3. 05	
2015. 8. 7	1. 36	1. 75	2015. 8. 6–8. 7	2. 00	1. 84	
2015. 8. 8	1. 89	2. 07	2015. 8. 7–8. 8	1. 55	1. 54	
2015. 8. 9	2. 01	2. 21	2015. 8. 8–8. 9	1. 77	1. 32	
2015. 8. 10	2. 24	2. 17	2015. 8. 9–8. 10	2. 07	1. 83	
2015. 8. 11	2. 80	2. 40	2015. 8. 10–8. 11	4. 81	3. 54	
2015. 8. 12	2. 11	1. 69	2015. 8. 11–8. 12	3. 11	1. 98	
2015. 8. 13	0. 78	0. 45	2015. 8. 13–8. 14	2. 27	1. 46	
2015. 8. 14	1. 80	1. 78	2015. 8. 14–8. 15	6. 21	3. 25	
2015. 8. 15	2. 58	2. 32	2015. 8. 15–8. 16	2. 32	1. 77	
2015. 8. 16	3. 61	3. 21	2015. 8. 16–8. 17	2. 10	1. 63	
2015. 8. 17	2. 76	2. 04	2015. 8. 17–8. 18	2. 43	2. 22	
2015. 8. 18	1. 42	1. 15	2015. 8. 18–8. 19	5. 66	2. 68	
2015. 8. 19	1. 86	1. 74	2015. 8. 19–8. 20	7. 75	3. 21	
2015. 8. 20	2. 54	2. 64	2015. 8. 20–8. 21	2. 59	2. 48	
2015. 8. 21	2. 14	2. 58	2015. 8. 21–8. 22	6. 46	3. 40	
2015. 8. 22	3. 29	2. 78	2015. 8. 22–8. 23	3. 50	2. 35	
2015. 8. 23	2. 27	2. 45	2015. 8. 23–8. 24	4. 65	2. 58	
2015. 8. 24	2. 15	2. 02	2015. 8. 24–8. 25	5. 65	4. 13	
2015. 8. 25	2. 67	2. 34	2015. 8. 25–8. 26	6. 10	4. 19	

956

957